ISSN 1027-4510, Journal of Surface Investigation: X-ray, Synchrotron and Neutron Techniques, 2020, Vol. 14, No. 2, pp. 359–365. © Pleiades Publishing, Ltd., 2020.
Russian Text © The Author(s), 2020, published in Poverkhnost', 2020, No. 4, pp. 49–56.

Blistering in Helium-Ion-Irradiated Zirconium, Aluminum, and Chromium Nitride Films

V. V. Uglov[a, b, *], G. Abadias[c], S. V. Zlotski[a, **], I. A. Saladukhin[a], A. A. Malashevich[a], A. L. Kozlovskiy[d, e], and M. V. Zdorovets[d, e]

[a] *Belarusian State University, Minsk, 220030 Republic of Belarus*
[b] *South Ural State University (National Research University), Chelyabinsk, 454080 Russia*
[c] *Prime Institute, University of Poitiers, Poitiers, 186000 France*
[d] *Engineering Profile Laboratory, Gumilyov Eurasian National University, Nur-Sultan, 010008 Kazakhstan*
[e] *Laboratory of Solid State Physics, Institute of Nuclear Physics, Almaty, 050032 Kazakhstan*
**e-mail: Uglov@bsu.by*
***e-mail: Zlotski@bsu.by*

Received August 15, 2019; revised September 17, 2019; accepted September 17, 2019

Abstract—This work is devoted to studying blistering in ZrN, AlN, and CrN films formed by reactive magnetron sputtering. The surface morphology and cross-sectional microstructure of mononitride films after irradiation with He ions (energy 40 keV and doses of 3×10^{17}–1.1×10^{18} cm^{-2}) at room temperature are analyzed by scanning, atomic force, and transmission electron microscopy. The critical doses of blistering are determined for ZrN (6×10^{17} cm^{-2}), AlN (5×10^{17} cm^{-2}), and CrN (6×10^{17} cm^{-2}) films. The high density of blisters in ZrN films leads to the merging of neighboring blisters (average size 0.75 μm) and the formation of large blisters (average size 1.35 μm). The blisters in the AlN films have a regular round shape (average size 1.7 μm). The CrN films are characterized by the presence of open blisters having a two-level structure: an upper blister with a diameter of 2–10 μm and a lower one with a diameter of 1.2 μm. As follows from the TEM results, 40-keV He-ion irradiation of the films and their subsequent vacuum annealing leads to the formation of chains of radiation-induced pores filled with helium in the region of the projective ion range R_p. The formation of extended cracks is found to occur in the R_p region of ZrN, which is caused by interbubble fracturing due to high excess pressure in pores located at a depth close to R_p.

Keywords: mononitride coatings, magnetron sputtering, radiation blistering, projective ion range, radiation effects

DOI: 10.1134/S1027451020020524

INTRODUCTION

The development of a new generation of nuclear reactors requires the creation of materials and coatings with a high radiation resistance [1–3]. The formation of blisters (defects on the surface of a material in the form of bubbles) during He-ion irradiation is one of the most important processes causing changes in the physical and chemical properties of the surface and a loss of structural integrity of the material, which eventually worsens the characteristics of the material itself [4–7]. Due to He-ion irradiation, blisters are formed in films (as well as bulk materials) because of the generation and growth of gas vacancy clusters. He inclusion into film soften leads to an increase in compressive stresses. Subsequent stress relaxation can be manifested as lamination (cracking) in the films, which results in film blistering or exfoliation (exfoliation of the film material without any visible deformation of the surface layer) [8, 9].

There are two models explaining blistering in materials: lateral stresses and interbubble fracture. In lateral stress models, blistering is explained by the penetration of gas atoms and the creation of interstitial atoms, vacancies, changes in the lattice parameters, and the formation of a disordered structure near the surface, which generates lateral stresses in the implanted region [10, 11]. The relaxation of these stresses during expansion of the blister cover makes a break in the metal corresponding to the bubble cavity.

The second model based on gas pressure suggests that blistering is initiated by a break occurring at a depth corresponding to the maximum concentration of implanted atoms. This break is explained by excessive growth of large gas blisters caused either by the association of helium-vacancy clusters or the merging of small blisters [12, 13]. Blistering becomes possible because helium and vacancies are combined into bubbles and tend to form large cavities parallel to the surface.

This work is devoted to studying the blistering process in He-ion irradiated ZrN, AlN, and CrN films (energy of 40 keV and doses of 5×10^{17}–1.1×10^{18} cm^{-2}) at room temperature.

EXPERIMENTAL

ZrN, AlN, and CrN coatings were deposited by magnetron sputtering in a vacuum chamber (basic pressure of $<10^{-5}$ Pa) equipped with cathodes (Zr, Al, Cr) and a cryogenic pump (maximum pumping rate of 500 L/s). The films were formed by sputtering Zr, Al, and Cr targets at temperatures of 300, 300, and 450°C respectively on single-crystal Si (100) substrates with a 10-nm-thick SiO_2 layer grown thermally. During the deposition a constant bias voltage of 60 V was applied to the substrate. The substrate was rotated with a speed of 15 rpm during deposition to provide an even thickness of the coating.

Water-cooled Zr, Al, Cr targets with a diameter of 7.62 cm were placed at a distance of 18 cm from the substrate holder. The coatings were deposited in an Ar + N_2 atmosphere. The Zr target was sputtered in an unbalanced magnetic-field configuration with a direct current source. Special attention was paid to the control of the surface state of the object before deposition with a multistage target-cleaning procedure. The partial N_2 pressure was measured and controlled during deposition by an MKS Microvision mass spectrometer.

The samples under study were irradiated with 40-keV He^{2+} ions and integral doses from 3×10^{17} to 1.1×10^{18} cm^{-2}. The energy parameters of irradiation were selected so that the distribution depth of implanted He impurities, which was calculated by the SRIM program, did not exceed the coating depth.

The mononitride films were additionally irradiated with 40-keV He^{2+} ions with an integral dose of 8×10^{17} cm^{-2} and annealed in vacuum (2×10^{-4} Pa) in a quartz tube furnace at 800°C for 2 h. An annealing temperature of 800°C was selected because it was 1/3 of the melting point of ZrN and AlN.

The surface morphology of the irradiated films was analyzed by scanning electron microscopy (SEM) on a LEO 1455 VP microscope and by atomic force microscopy (AFM) on a Solver P47 Pro scanning probe microscope.

The microstructure of cross sections of the deposited coatings was analyzed by high-resolution transmission electron microscopy (HR-TEM) on a JEOL JEM 2100 microscope at an accelerating voltage of 200 kV. Samples were prepared for TEM analysis by a focusing ion beam (FIB) using an FEI Helios Nanolab 650 instrument.

RESULTS AND DISCUSSION

X-ray crystallography analysis showed that the mononitride coatings (ZrN, CrN, AlN) obtained by reactive magnetron sputtering had a polycrystalline structure. Their phase composition is characterized by the presence of crystalline ZrN, CrN, and AlN phases with a preferred orientation of (111), (200), and (002) respectively. The results of a phase composition similar to the obtained ones are also presented in [14–16]. The elemental-analysis results revealed that the composition of mononitride films was close to the stoichiometric one (Zr 44.3 at % and N 55.7 at % for ZrN; Al 43.6 at % and N 56.4 at % for AlN; Cr 54.6 at % and N 45.4 at % for CrN).

The ZrN, AlN, and CrN films were irradiated with He ions (40 keV) in the dose range from 3×10^{17} to 1.1×10^{18} cm^{-2}. The typical calculated concentration profiles of implanted He and a damaging dose for CrN and ZrN are shown in Figs. 1a, 1c. The average projective He range in ZrN, AlN, and CrN was 158 ± 58, 267 ± 53, and 165 ± 51 nm respectively.

The radiation-induced erosion of 40-keV He-ion irradiated ZrN, AlN, and CrN films was examined by SEM. It is found that irradiation with doses up to 5×10^{17} cm^{-2} does not cause radiation erosion of the surface of the mononitrides. Figure 2 presents SEM images of the surface of the mononitride films irradiated with He-ion doses of 5×10^{17} and 6×10^{17} cm^{-2}. It is seen that open and closed blisters formed on the surface.

The analysis of SEM data on mononitride films irradiated with 40-keV He ions in the dose range from 3×10^{17} to 1.1×10^{18} cm^{-2} allowed us to experimentally determine the critical doses of blistering (the doses at which radiation erosion of the surface starts), which were 6×10^{17} cm^{-2} for the ZrN and CrN films and 5×10^{17} cm^{-2} for the AlN film. From Fig. 2 it is seen that there are significant differences in the blistering features for various types of mononitride films. In the case of ZrN and AlN films, closed blisters are observed (Figs. 2a, 2b). Cracks are seen on the surface of the AlN films, which appear due to the fact that the pressure in the blister cavity surpasses the ultimate tensile strength of the AlN films.

Estimation of the blister density on the surface of the ZrN and AlN films reveals that the blister density for ZrN films (5.3×10^7 cm^{-2}) exceeds this value for AlN films (1.3×10^7 cm^{-2}). As seen from Fig. 1a, the occurrence of a high blister density in ZrN films causes both the merging of small neighboring blisters (the average size is 0.75 μm) and the formation of a new large blister (the average size is 1.35 μm) with an irregular shape. Thus, two groups of blisters form on the surface of ZrN films: small and large. In AlN films, the blisters have a regular round shape (the average size is 1.7 μm).

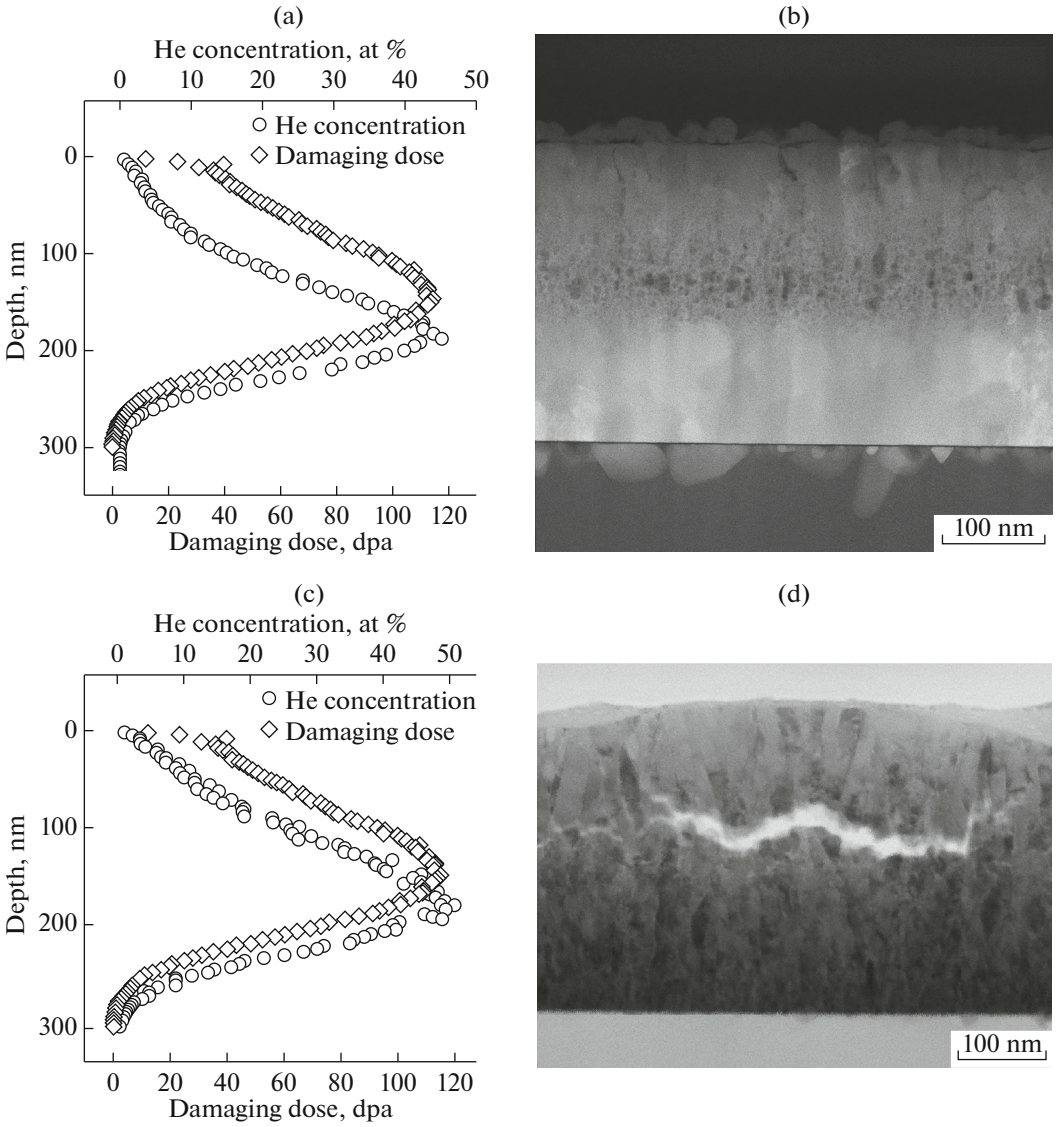

Fig. 1. Distribution profiles of implanted He and the damaging dose in CrN (a) and ZrN (c) films. TEM images of the cross section of CrN (b) and ZrN (d) films irradiated with He ions (40 keV, 8×10^{16} cm^{-2}) and annealed at 800°C.

Unlike the ZrN and AlN films, mainly open blisters as well as a small number of closed ones are present on the CrN surface (Fig. 2b). The blister sizes range from 2 to 10 μm, which substantially exceeds the values for ZrN and AlN films. Figure 3 presents AFM images of the surface of the CrN film and its profile. According to the SEM and AFM data, large open blisters are observed on the CrN surface whose boundaries mainly contain small blisters with a diameter of 1.2 μm (Figs. 2c and 3a). The depth of a large blister is about 75 nm and that of a small one is 110–150 nm. The total depth of the blisters is comparable with R_p (190 nm). The formation of this structure of blisters seems to be related to the heterogeneous depth distribution of chromium in the CrN film. This leads to the formation of a more fragile near-surface layer as compared to the main film. As a result of He-ion irradiation, a gas pore with overpressure and a diameter of 1.2 μm forms in the film at the depth R_p, which correlates with the He-ion range depth. During blistering (surface bulging) the erosion mechanism changes to the exfoliation of a 75-nm layer (the surface layer is more fragile) in association with a small blister [17]. The association of blisters forms a large blister whose cover is destroyed by a mechanism (periphery breaking) characteristic of fragile materials.

The high blister density in ZrN and AlN films is likely to be due to the low mobility of radiation-induced helium-vacancy clusters, which leads to a high density of gas pores at the He-ion range depth. For the CrN film the mobility of defects is higher,

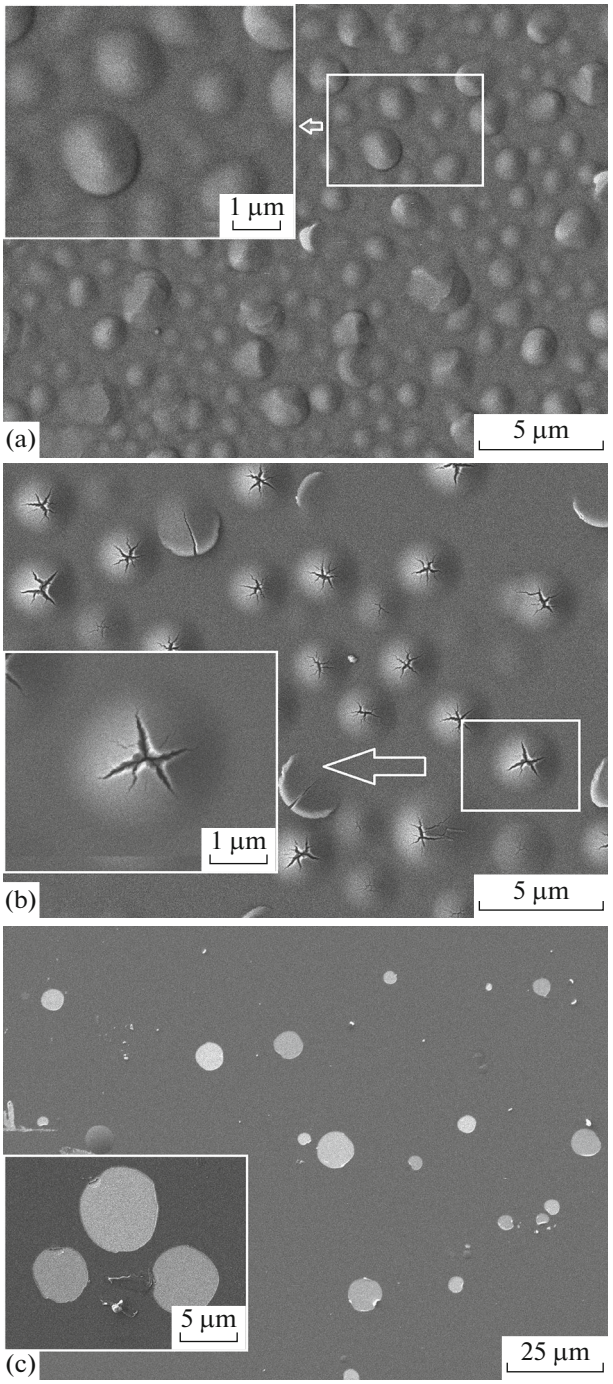

Fig. 2. SEM images of the surface of ZrN (a), AlN (b), and CrN (c) films irradiated with He ions (40 keV) at doses of 5×10^{17} (b) and 6×10^{17} cm^{-2} (a, c). The insets show SEM images of the film surface at a larger magnification.

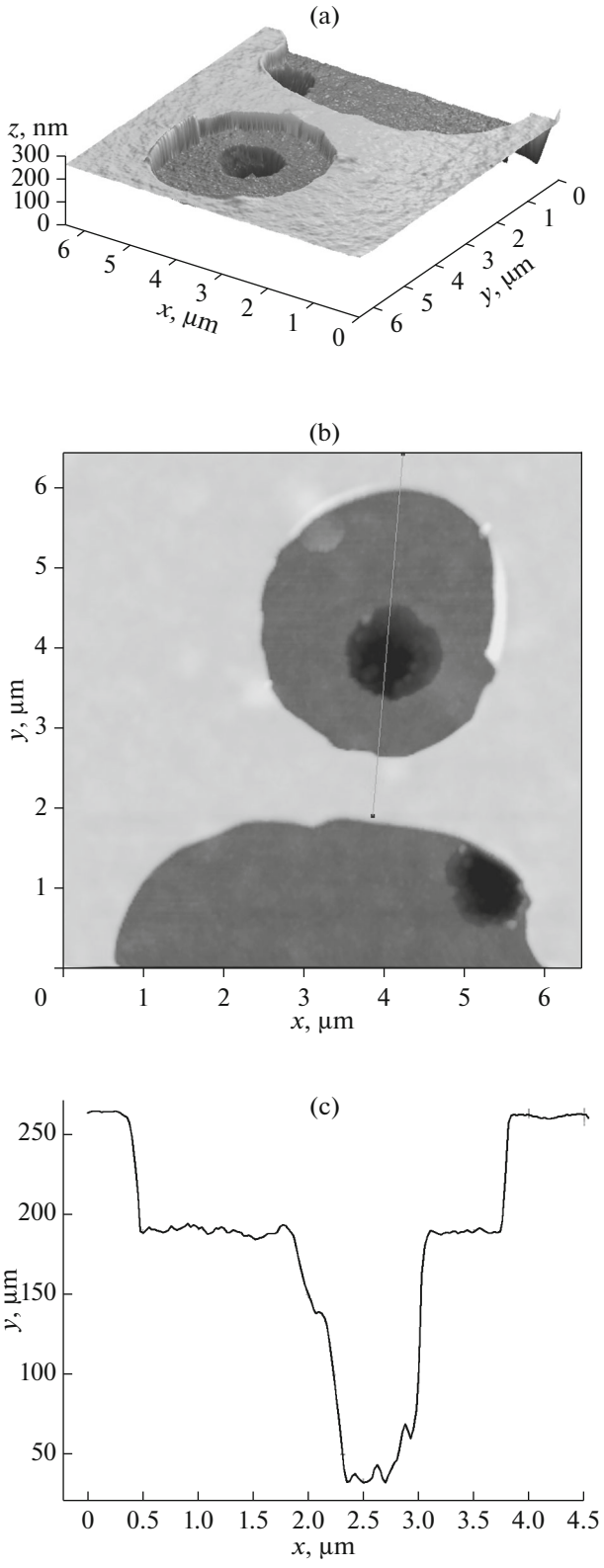

Fig. 3. AFM images of the surface of the 40-keV He-ion irradiated CrN film with a dose of 6×10^{17} cm^{-2}: (a) 3D image; (b) 2D image; (c) distribution-line profile shown in the 2D image.

which along with a variable structural phase state near the surface and in the film depth, causes blurring of the pore chain perpendicular to the film surface (Fig. 1b).

To estimate the radiation resistance of mononitride films, we calculated their surface erosion (as the ratio

of the area occupied by blisters to the film surface) depending on the radiation dose (Fig. 4).

As shown in Fig. 4, when the radiation dose increases, a tendency toward growth of the degree of surface erosion is observed in the CrN film. For this mononitride surface erosion is much lower than that for ZrN and AlN. In the AlN film, surface erosion increases up to a radiation dose of 6×10^{17} cm^{-2}. Surface erosion does not increase with a further increase in the radiation dose. The degree of surface erosion of the ZrN films barely changes and remains large (about 91%). An increase in the degree of surface erosion is due to the formation of additional bubbles with overpressure among which interbubble fracture occurs later and a gas cavity forms, causing the appearance of new blisters on the film surface. In the case of a high blister density, when the distance between blisters corresponds to its diameter, the further formation of new blisters is impossible because of the absorption of helium-vacancy clusters formed by the existing pores.

An increase in the radiation dose also results in an increase in the number of large blisters in ZrN films, which is due to the merging of neighboring blisters. No increase in the blister size is observed here. An increase in the radiation dose, and correspondingly, pressure in blisters results in their fracture (appearance of cracks on the blister cover) at a radiation dose of 7×10^{17} cm^{-2}. An increase in the radiation dose also does not cause the growth of grain sizes in CrN films because already at a dose of 5×10^{17} cm^{-2} the blister cover is destroyed (Fig. 2c). An increase in the average blister diameter from 1.8 to 2.3 μm with increasing radiation dose was revealed only for the AlN film. It correlates with an increase in the degree of mononitride surface erosion.

The TEM results for cross sections of ZrN and CrN films with the respective He-concentration distributions over the film depth, which were calculated by SRIM-2008, are illustrated in Fig. 1.

Microscopic studies of the cross sections of CrN and ZrN films were performed for systems successively irradiated with He ions (40 keV, dose 5×10^{16} cm^{-2}) and annealed in vacuum at 600°C. Annealing was conducted to accelerate the formation of gas pores.

The TEM results (Fig. 1b) indicate that the He-ion irradiation of CrN films causes the formation of helium-filled pores. It is seen that the diameter of radiation pores increases as the film depth approaches the R_p region and this region of pore formation is about 150 nm. The results of the He-concentration distribution over the irradiated film depth, which were calculated by SRIM-2008, show that the largest diameter of the radiation-induced pores is in the R_p region. This indicates the occurrence of gas overpressure in the pores located in this region.

Based on the above results, it can be assumed that the formation of extended cracks in the R_p region (Fig. 1d) is due to interbubble fracture caused by high overpressure in the pores located at depths close to R_p.

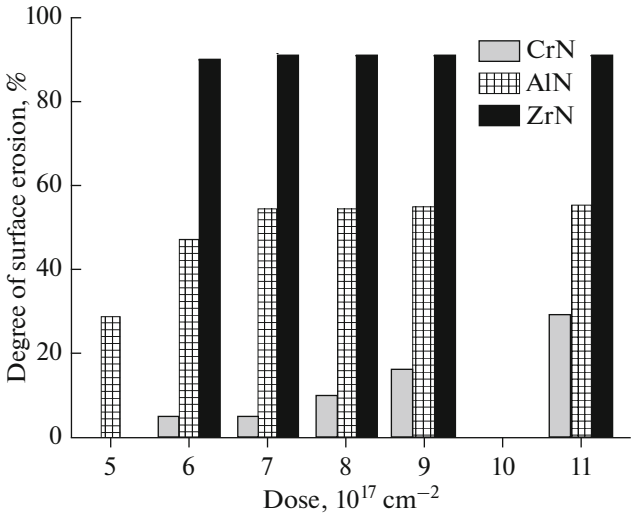

Fig. 4. Dependence of the degree of erosion of the surface of mononitride films on the He-ion irradiation dose (40 keV).

The interbubble-fracture mechanism was first proposed by Evans and described in [13]. In accordance with this mechanism, blistering consists of several stages. The stages of blister development in accordance with the Evans interbubble-fracture mechanism are presented in Fig. 5.

At the first stage, He embedding leads to the formation of bubbles of excessive pressure. At some critical He dose and some critical depth from the surface a bubble layer can have enough pressure to merge because of interbubble fracture and produce an internal crack. The bubble pressures are assumed to vary in a wide range with a maximum appearing in the R_p layer where the internal pressure equals that needed for interbubble fracture. This assumption is confirmed by TEM results (Fig. 1d).

At the second stage, the tensile stress created near the crack is directed perpendicular to the crack plane, and consequently, tends to expand this plane.

At the third stage, if the overpressure of bubbles in the adjacent layers to the crack is much higher than the pressure in the crack, then this difference can be high enough for each separate bubble to fracture into a crack, i.e., each bubble will act as a microblister. The common result is crack expansion due to increasing overpressure in it. This process can be repeated and involve several layers of bubbles adjacent to the crack. The process stops when the gas-pressure difference in the crack and the adjacent bubbles to the crack is insufficient for the formation of microblisters.

At the fourth stage, until this "unzipping" process (stage 3) of the bubble layers continues, the pressure in

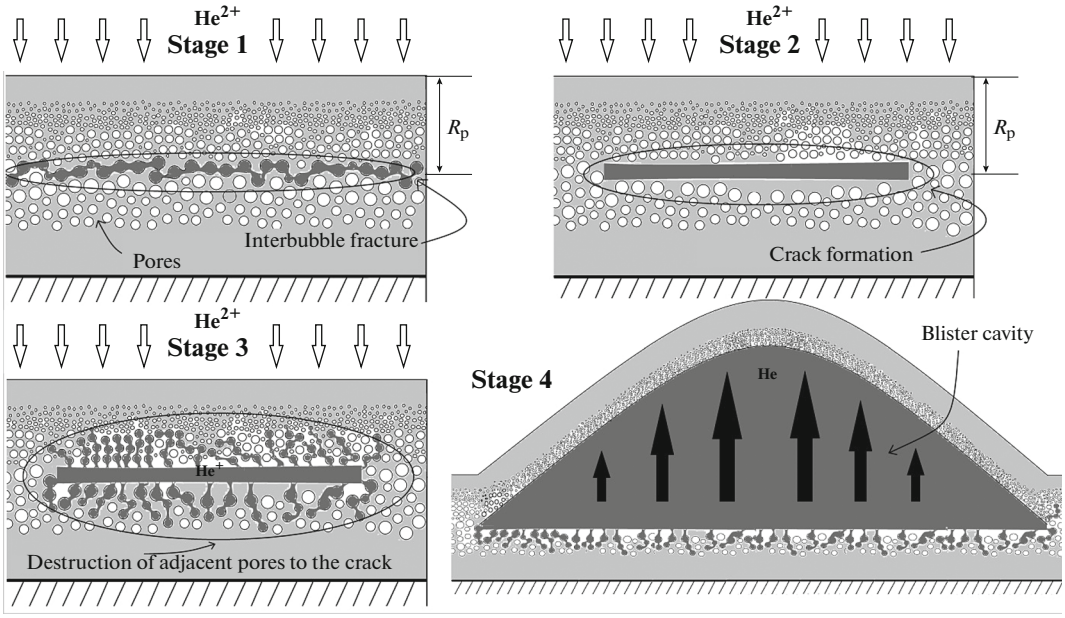

Fig. 5. Stages of blistering in He-ion irradiated films.

the crack may be enough to begin the deformation of the material layer above the crack.

Blistering in ZrN, CrN, and AlN films is well described within the model of interbubble fracture.

Current studies of blistering in ion-irradiated materials show that a microcrack-cavity can form due to the association (coalescence) of bubbles and the development of an interbubble crack. Subsequent destruction of the surface layer occurs under the impact of gas pressure inside the cavity in the presence of internal compressive stresses arising in the implanted layer and stabilizing the motion of the crack [18]. Evolution of this approach proceeded by developing and combining the models of lateral stresses, gas pressure, and interbubble fracture.

Thus, blistering is the result of the combined effect of microstresses caused by gas overpressure in bubbles and lateral compressive macrostresses due to swelling of the irradiated layer, with the key role being played by the gas pressure. The blister nuclei are nanoscale (diameter of 1–4 nm) gas bubbles with overpressure that associate into gas cavities. The mechanism of gas association (coalescence or the formation of an interbubble crack) depends on the irradiation temperature and mechanical properties of the material [18].

CONCLUSIONS

The He-ion irradiation (40 keV) of mononitrides leads to the formation of closed blisters in AlN and ZrN films at doses of 5×10^{17} and 6×10^{17} cm^{-2} and double-layered open blisters in a CrN film at a dose of 6×10^{17} cm^{-2}.

The high blister density in ZrN films results in the merging of neighboring blisters (average size of 0.75 μm) and the formation of large blisters (average size of 1.35 μm). The blisters in the AlN films have a regular round shape (average size of 1.7 μm).

It is found that the radiation-induced erosion in CrN films (unlike ZrN and AlN films) is characterized by the occurrence of open blisters with a double-layered structure: an upper blister with a diameter of 2–10 μm and a lower one with a diameter of 1.2 μm. The formation of a double-layered structure of blisters is related to the depth distribution of chromium which causes the formation of a fragile layer near the film surface. Radiation-induced erosion of the surface of the ZrN films is 90%; that of the AlN film is 29% and linearly increases to 55% (7×10^{17} cm^{-2}); and that of CrN increases from 5 to 29%, which is mainly due to the mobility of helium-vacancy complexes in the films.

It is revealed that chains of He-filled radiation pores form in the R_p region in He-ion irradiated CrN films annealed at 600°C. The formation of extended cracks in the R_p region in He-ion irradiated ZrN annealed at 600°C is also revealed. The formation of cracks is explained by interbubble fracture caused by high overpressure in pores located at depths close to R_p.

FUNDING

The work was supported by the Belorusian Foundation for Basic Research (project no. F18MS-027).

REFERENCES

1. S. J. Zinkle and G. S. Was, Acta Mater. **61,** 735 (2013).

2. V. V. Uglov, G. Abadias, and S. V. Zlotski, J. Surf. Invest.: X-Ray, Synchrotron. Neutron Tech. **9** (5), 995 (2015).
3. A. Janse van Vuuren, J. H. Neethling, and V. A. Skuratov, Nucl. Instrum. Methods Phys. Res., Sect. B **326,** 19 (2014).
4. S. Agarwal, P. Trocellier, and Y. Serruys, Nucl. Instrum. Methods Phys. Res., Sect. B **327,** 117 (2014).
5. S. J. Zinkle, Nucl. Instrum. Methods Phys. Res., Sect. B **286,** 4 (2012).
6. V. V. Uglov, *Radiation Processes and Phenomena in Solids* (Vysheishaya shkola, Minsk, 2011), p. 207 [in Russian].
7. V. V. Uglov, *Radiation Processes and Phenomena in Solids* (Vysheishaya shkola, Minsk, 2011), p. 188 [in Russian].
8. Z. J. Liu, N. Jiang, Y. G. Shen, and X. N. Li, Thin Solid Films **516,** 7609 (2008).
9. M. Y. He and A. G. Evans, Mater. Sci. Eng. **245,** 168 (1998).
10. J. H. Evans, J. Nucl. Mater. **76–77,** 228 (1978).
11. E. P. EerNiss and S. T. Picraux, J. Appl. Phys. **48** (1), 9 (1977).
12. W. G. Wolfer, J. Nucl. Mater. **93–94,** 713 (1980).
13. J. H. Evans, J. Nucl. Mater. **68,** 129 (1977).
14. G. Abadias, V. V. Uglov, I. A. Saladukhin, S. V. Zlotski, et al., Surf. Coat. Technol. **308,** 158 (2016).
15. T. A. Kuznetsova, V. A. Lapitskaya, S. A. Chizhik, V. V. Uglov, et al., IOP Conf. Ser.: Mater. Sci. Eng. **443** (012018), 5 (2018).
16. W. Siriprom, C. Chananonnawathorn, S. Kongsriprapan, K. Teanchai, et al., Mater. Today: Proc. **5,** 15224 (2018).
17. A. S. Kuznetsov, M. A. Gleeson, and F. Bijkerk, J. Phys.: Condens. Matter **24,** 052203 (2012).
18. E. G. Grigor'ev, Yu. A. Perlovich, G. I. Solov'ev, A. L. Udovskii, and V. L. Yakushin, *Physical Materials Science, Vol. 4: Physical Principles of Strength. Radiation Physics of the Solid State. Computer Simulation* (Mosk. Inzh. Fiz. Inst., Moscow, 2008) [in Russian].

Translated by L. Chernikova